JOURNAL OF AIRCRAFT
Vol. 39, No. 2, March–April 2002

Prediction of Airfoil Stall in Icing Conditions Using Wing Surface Pressures

Arthur Hoadley* and Erik Pederson†
Western Michigan University, Kalamazoo, Michigan 49008

Initial work is presented on an in-flight stall margin instrumentation system that maintains accuracy independent of wing leading-edge ice formations. The system uses four surface pressures, measured aft of the ice formation, from which the aircraft's normalized lift coefficient is determined. The pressure port locations are selected such that the calibration algorithm remains nearly constant as the leading-edge ice shape and thickness change. Wind-tunnel data are presented for three ice formations, varying in both type and thickness. The indicated normalized lift coefficient, based on the no ice algorithm, is compared to the actual normalized lift coefficient under icing conditions. From this comparison, the four port locations were found to be located at 22 and 41% of the chord on the upper wing surface and 41 and 68% on the lower wing surface.

Nomenclature

C_L	=	lift coefficient
$C_{L\max}$	=	maximum lift coefficient
C_{LN}	=	normalized lift coefficient
$C_{L\alpha}$	=	lift curve slope
Cp	=	standard pressure coefficient
Cp_x	=	pseudopressure coefficient from the instrumentation
α	=	angle of attack
α_s	=	stall angle of attack
δ_f	=	flap deflection angle

Introduction

AN airplane's stall margin (SM) can be defined as the percentage of the airplane's lift coefficient C_L remaining to be used, as shown in Eq. (1). The normalized lift coefficient C_{LN} is defined in Eq. (2). When SM is 100%, the aircraft has its entire lift coefficient available for use. When SM is 0%, the aircraft has none of its lift coefficient available, and the aircraft has reached stall[1,2]:

$$\mathrm{SM} = (1 - C_{LN}) \cdot 100\% \tag{1}$$

$$C_{LN} = C_L / C_{L\max} \tag{2}$$

Currently available cockpit instrumentation systems display a normalized angle of attack, or require the pilot to adjust manually the airplane's approach speed based on flight manual data combined with the calculated aircraft weight and flap configuration. The accuracy of these systems is dependent on calibrations performed for known configuration changes, such as wing flaps. Changes in the wing airfoil shape due to ice formation are not accounted for in the system calibrations and are, therefore, errors. If an airplane accumulates significant ice, the actual SM will decrease with no indicated change in the cockpit. As the actual SM approaches zero, the airplane will have a reduction in its performance and control margins. If the aircraft is being flown by an autopilot, these reduced margins most likely will go undetected by the flight crew. If the pilot and autopilot have accurate SM data, the ice formation can be detected early, allowing the crew to respond in a timely manner.

Received 31 January 2001; revision received 15 May 2001; accepted for publication 6 August 2001.

*Professor, Department of Mechanical and Aeronautical Engineering.
†Graduate Student, Department of Mechanical and Aeronautical Engineering.

This paper presents initial work on an in-flight SM instrumentation system that maintains accuracy in spite of wing leading-edge ice formations. The system uses four surface pressures, measured aft of the ice formation, from which the aircraft's normalized lift coefficient C_{LN} is determined. The pressure port locations are selected such that the calibration algorithm remains nearly constant as the leading-edge ice shape and thickness change. A two-dimensional airfoil pressure model was used to obtain the surface pressure distribution for a range of angles of attack and ice formations. Analysis of the data has identified port locations that provide C_{LN} data within 11% of the actual value, with and without ice. The initial data were collected using an airfoil approximating a NACA 0018 because this model was readily available. A software package, LEWICE, was obtained from NASA John H. Glenn Research Center and was used to predict four ice shapes. These shapes were cut from a foam block, using a hot wire, and attached to the model leading edge for testing. These initial experiments have shown great promise, but the concept needs to be duplicated on an airfoil more commonly used for wings and more ice shapes also need to be tested.

Explanation of Theory

SM is defined as a function of normalized lift coefficient C_{LN}, as shown in Eqs. (1) and (2). For the system being presented in this paper, C_{LN} will be determined from a defined pressure coefficient Cp_x. Cp_x is defined in Eq. (3), where $P1$, $P2$, $P3$, and $P4$ are wing surface pressures, measured at four different port locations. By substitution, the Cp_x can also be written in terms of the wing surface pressure coefficients.[1,2] Given that Cp is a function of angle of attack α, flap deflection δ_f, ice shape (IS), and port location (PL), then it follows that Cp_x will also be a function of these parameters,

$$Cp_x = \frac{P1 - P2}{P3 - P4} = \frac{Cp1 - Cp2}{Cp3 - Cp4} \tag{3}$$

$$Cp_x = f_1(\alpha, \delta_f, \mathrm{IS}, \mathrm{PL}) \tag{4}$$

An example of the PLs is shown in Fig. 1. $C_{LN\text{-actual}}$ is defined in Eq. (5), where α_s is the stall angle of attack for the airfoil configuration. $C_{LN\text{-indicated}}$ is related to $C_{LN\text{-actual}}$ through the calibration function (f_2) of Cp_x and flap deflection, as is shown in Eq. (6):

$$C_{LN\text{-actual}} = \frac{C_{L\alpha} \cdot \alpha}{C_{L\alpha} \cdot \alpha_s} = \frac{\alpha}{\alpha_s} \tag{5}$$

$$C_{LN\text{-indicated}} = f_2(Cp_x, \delta_f) \Leftrightarrow C_{LN\text{-actual}} \tag{6}$$

Let Cp_{x0} be defined as Cp_x in the calibration configuration, as shown in Eq. (7). The calibration configuration is the wing configuration when there are no ice formations:

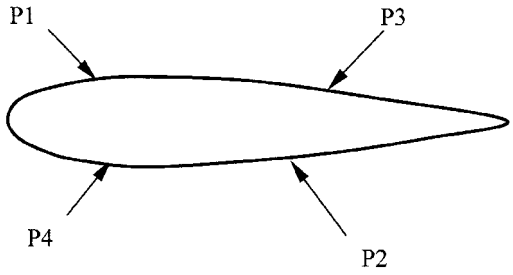

Fig. 1 Pressure PLs.

$$Cp_{x0} = f_1(\alpha, \delta_f, \text{IS} = 0, \text{PL}) = f_1(\alpha, \delta_f, 0, \text{PL}) \tag{7}$$

In the calibration configuration, $C_{LN\text{-actual}}$ is equal to $C_{LN\text{-indicated}}$, and both are equal to a function f_2 of Cp_{x0} and flap deflection, as is shown in Eq. (8). Note that the function of flap deflection is a first-order effect and needs to be considered in the baseline calibration (f_2):

$$C_{LN\text{-actual}} = C_{LN\text{-indicated}} = f_2(Cp_{x0}, \delta_f) \tag{8}$$

Function f_2 generally has a second-order form, as shown in Eq. (8a):

$$f_2(Cp_{x0}, \delta_f) = A_0(\delta_f) + A_1(\delta_f) \cdot Cp_{x0} + A_2(\delta_f) \cdot (Cp_{x0})^2 \tag{8a}$$

The data presented in Fig. (2) are relatively linear, but this is not necessarily the case for all acceptable PLs.

As ice is accumulated, the wing configuration changes and $C_{LN\text{-indicated}}$ is no longer a function of Cp_{x0} alone. It can now be expressed as a new function f_3 of the IS, flap deflection angle, and Cp_{x0}, as

$$C_{LN\text{-indicated}} = f_3(Cp_{x0}, \text{IS}, \delta_f) \tag{9}$$

Now let the function f_3 have the form

$$C_{LN\text{-indicated}} = \frac{m_1(\delta_f, \text{IS}, \text{PL})}{m_2(\delta_f, \text{IS}, \text{PL})} \cdot f_4[Cp_{x0}, \delta_f] \tag{10}$$

where Cp_{x0} is a function f_1 of only angle of attack, flap deflection, and PL. The new functions m_1 and m_2 are functions of only flap deflection, IS, and PL.

Note that the function of flap deflection in m_1 and m_2 is a second-order effect because the baseline flap effects have been accounted for in the calibration function f_4. When it is assumed that PLs can be selected such that functions m_1 and m_2 are equal, this equation can be rewritten, as

$$C_{LN\text{-indicated}} = f_4(Cp_{x0}, \delta_f) \tag{11}$$

where $C_{LN\text{-indicated}}$ is only a function of Cp_{x0}.

Because $C_{LN\text{-indicated}}$ is only a function of Cp_{x0} and flap deflection in both Eqs. (8) and (11), functions f_2 and f_4 must be equal,

$$f_2(Cp_{x0}, \delta_f) = f_4(Cp_{x0}, \delta_f) \tag{12}$$

Because both $C_{LN\text{-indicated}}$ and $C_{LN\text{-actual}}$ are equal to f_2 and f_2 equals f_4, then $C_{LN\text{-indicated}}$ with ice must equal $C_{LN\text{-actual}}$,

$$C_{LN\text{-actual}} = C_{LN\text{-indicated}} \tag{13}$$

Given the assumptions as to the form of f_3, and the selected PLs that make m_1 and m_2 equal, $C_{LN\text{-indicated}}$ is equal to $C_{LN\text{-actual}}$ independent of ice shape and flap deflection.

Actual Conditions

Under actual flight conditions there will be deviations from the assumptions made in the theory. The indicated C_{LN} may not be totally independent of the ice shape or flap deflection. There will be some error related to the ice, Er_1 and some error related to the second-order flap deflection, Er_2,

$$C_{LN\text{-indicated}} = C_{LN\text{-actual}} + Er_1(\text{IS}) + Er_2(\delta_f) \tag{14}$$

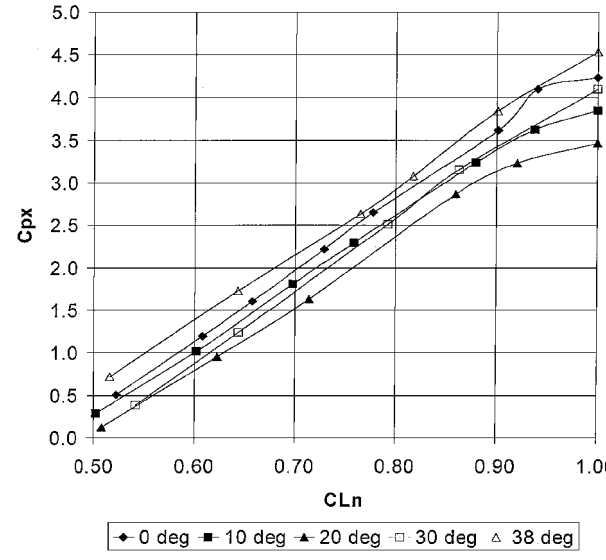

Fig. 2 Cessna 182 SM flight-test data.

Figure 2 presents data from an SM system installed on Western Michigan University's flight-test aircraft. Each curve is Cp_x vs C_{LN} curves for a different flap angle setting. The ports were located on this airplane to maximize the sensitivity of Cp_x to changes in C_{LN} and not to compensate for flap deflection.[1,2] The current system uses a multivariate calibration similar to the one presented in Eq. (8a). If the calibration function were to ignore the effect of flap deflection, a C_{LN} error of 6% would result. Note that flap deflection angles are repeatable. This repeatability allows a different calibration to be used for each setting, which will minimize $Er_2(\delta_f)$.

The error due to ice shape cannot be removed by this method because of the nonrepeatable characteristic of ice formations. Aircraft icing is a random phenomenon and, therefore, has to be compensated for through other means. The method presented in this paper minimizes the effect of ice by the careful selection of the pressure sensor PLs. Computational methods of analysis have difficulty predicting the pressure coefficients at high angles of attack with horned ice shapes. They will also have difficulty determining the stall angle of attack. For these reasons, an experimental approach was taken to evaluate the proposed theory.

Experimental Method

A 12-in. chord pressure model, which approximated an NACA 0018 airfoil, was adapted for the Western Michigan University Advanced Design Wind Tunnel (ADWT). The model spanned the entire 42-in. test section. This was done to eliminate three-dimensional effects on the wing, thereby simulating two-dimensional flow. The model had 20 pressure ports on the upper wing surface and 20 ports on the lower wing surface.

The wind tunnel at Western Michigan University is not capable of producing ice; thus, another method had to be developed to predict and model the ice shapes. For this purpose, a computational ice simulation software package, LEWICE, developed at NASA John H. Glenn Research Center, was used.[3] This software uses computational panel methods to predict the ice shape that forms on a surface. This shape is based on the angle of attack, temperature, airspeed, water droplet size, and time in the icing situation. Figure 3 shows the different shapes used in this test. Each ice shape was formed using the same airspeed, droplet size, and angle of attack, while varying the temperature and duration in the icing conditions. These parameters were used to simulate an aircraft in a cruise flight configuration. Table 1 shows the parameters used to produce each ice shape. Both horned and smooth ice shapes were modeled; however, configuration 1 was not tested due to model vibration problems. For the baseline wing configuration, and configurations 2–4, surface pressure data were collected over a range of angles of attack. The ports under the ice formation were not used because they may not be available under actual icing conditions. Each configuration was tested multiple times to test for repeatability. The Cp vs x/c was

Table 1 Parameters for ice shape formation

Parameter	$C1$	$C2$	$C3$	$C4$
Temperature, °C	−4.85	−17.8	−17.8	−4.85
Airspeed, m/s	72	72	72	72
Angle of attack, deg	3	3	3	3
Droplet size, mm	20	20	20	20
Time in flow, s	600	1200	600	300
Pressure at infinity, N/m^2	100,000	100,000	100,000	100,000
Relative Humidity, %	100	100	100	100
LWC, gm/m^3	0.54	0.54	0.54	0.54

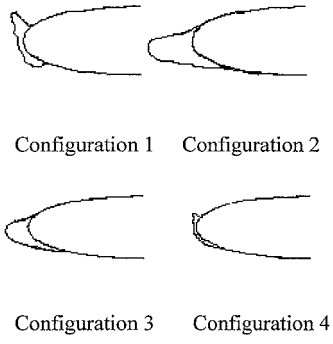

Fig. 3 Computationally determined ice shapes.

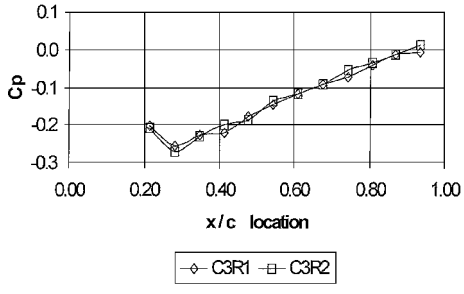

Fig. 4 Configuration 3 repeatability test for 4-deg angle of attack.

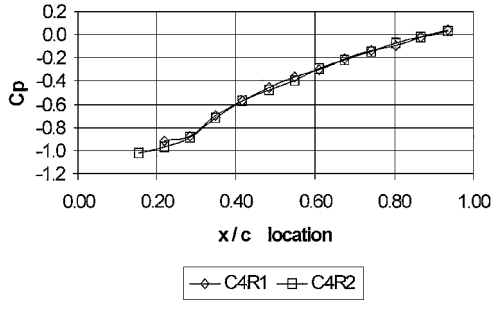

Fig. 5 Configuration 4 repeatability test for 4-deg angle of attack.

compared for each run to determine the repeatability of the data. A sample of this comparison is shown in Figs. 4 and 5. The data were determined to be repeatable, and the analysis was continued.

To determine C_{LN}, the stall angle of attack for each ice configuration needed to be known. The pressure model produced too great a load for the available wind-tunnel balance, and the pressure tubing would have interfered with the balance. Thus, the stall angle of attack could not be determined from force data. Tufts, placed on the wing upper surface at several chord locations, were observed to determine at what angle of attack the flow separated. For this series of experiments, a flow separation at 50% of the chord was considered to be stalled. When the stall angle of attack was known, the C_{LN} could be determined for each angle of attack and ice formation tested. The stall angles of attack for each configuration are listed in Table 2.

A nontrivial Cp_x was computed for each combination of the pressure ports not located under the ice formation. To qualify for consideration, the relationship between Cp_x and C_{LN}, between a C_{LN} of 0.5 and 1.0, was examined. This range of C_{LN} represents the normal landing and takeoff values. The slope of the C_{LN} vs Cp_x curve was required to be greater than a minimum threshold to ensure sufficient sensitivity to changes in C_{LN}. The port sets that met this criterion were compared against the other ice shapes and the baseline data.

Table 2 Stall angles of attack

Configuration	Stall angle of attack, deg
No ice	9
2	4.8
3	5
4	6

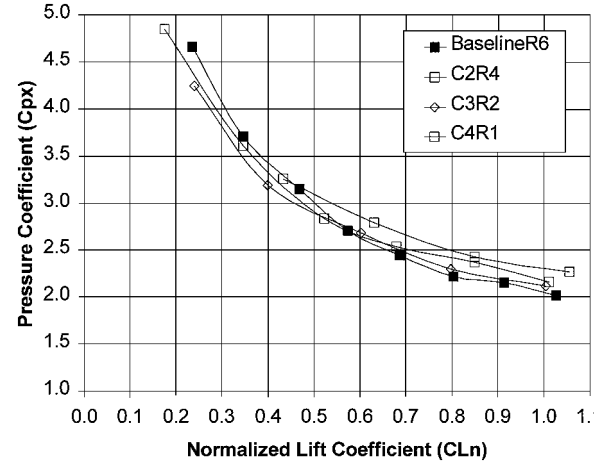

Fig. 6 Cp_x vs C_{LN} for selected PLs.

Experimental Results

This analysis yielded a set of PLs that maintained nearly the same relationship, regardless of ice configuration. The x/c locations for this set of ports are for upper wing surface $P1(x/c = 0.22)$ and $P3(x/c = 0.41)$ and for lower wing surface $P2(x/c = 0.68)$ and $P4(x/c = 0.41)$.

The pressures measured at these ports are combined to give Cp_x:

$$Cp_x = (P1 - P2)/(P3 - P4) \tag{15}$$

Figure 6 shows the C_{LN} vs Cp_x relationship for this set of ports. The relationship is shown for the no ice baseline and ice configurations (2–4), which are labeled C2R4, C3R2, and C4R1, respectively.

Error Analysis

Figure 6 shows that for a given Cp_x there is a C_{LN} error of around 11% between the four curves. An uncertainty analysis was done on the data for these ports to see if the uncertainty in the measurements explained the 11% error. Figure 7 shows the same graph as in Fig. 6, but this time the uncertainty for the baseline is also shown. The baseline uncertainty was plotted because the baseline curve is the calibration that would be used for the actual instrumentation. If all of the ice configuration data fell within this baseline uncertainty, then the error in each port reading would be due to instrumentation error and would not be due to ice configuration. The uncertainty for the baseline configuration encompasses most of the data from the other configurations, with some exceptions at higher normalized lift coefficients. To lessen the uncertainty further, pressure data would need to be taken at a higher dynamic pressure Q. It was not possible to take data at a higher Q due to the lack of structural integrity of the pressure model. Initially, the 11% error would be acceptable because the C_{LN} indicated to the pilot would be better than no indication at all. Ideally, the error would need to be in the ±2% range.

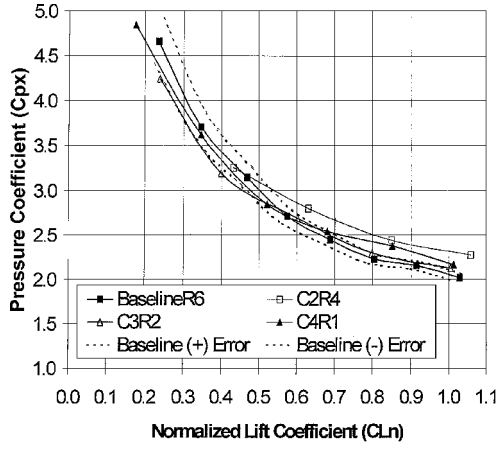

Fig. 7 Cp_x **vs** C_{LN} **for the selected PLs with baseline error.**

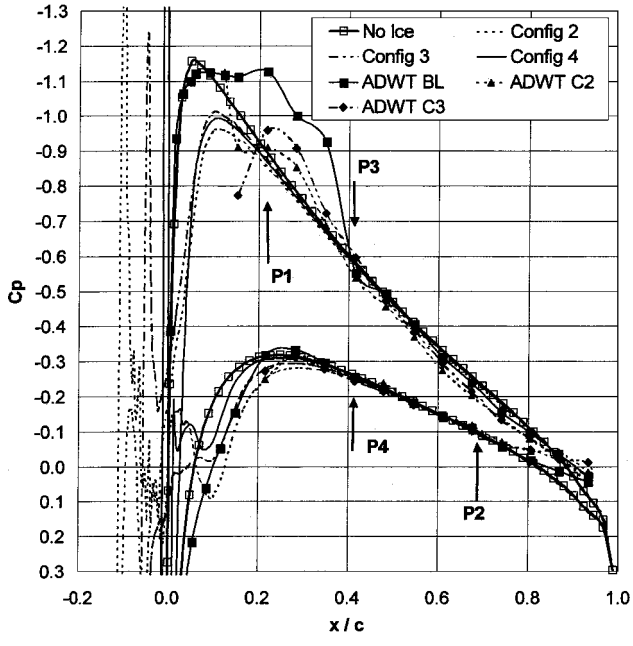

Fig. 8 LEWICE *Cp* **distributions for 3-deg angle of attack.**

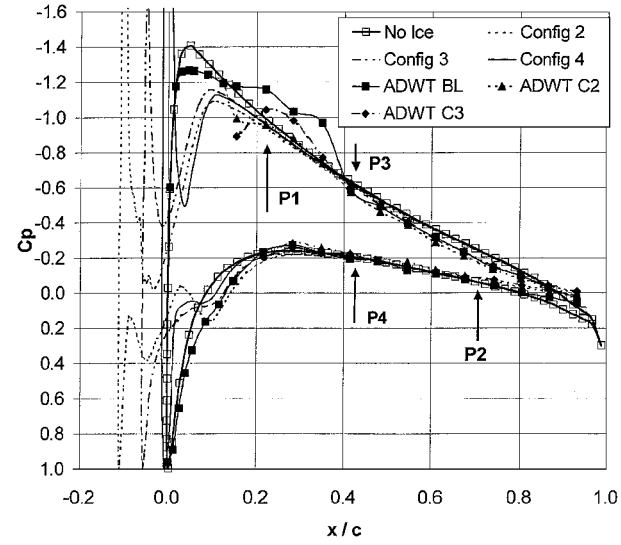

Fig. 9 LEWICE *Cp* **distributions for 4-deg angle of attack.**

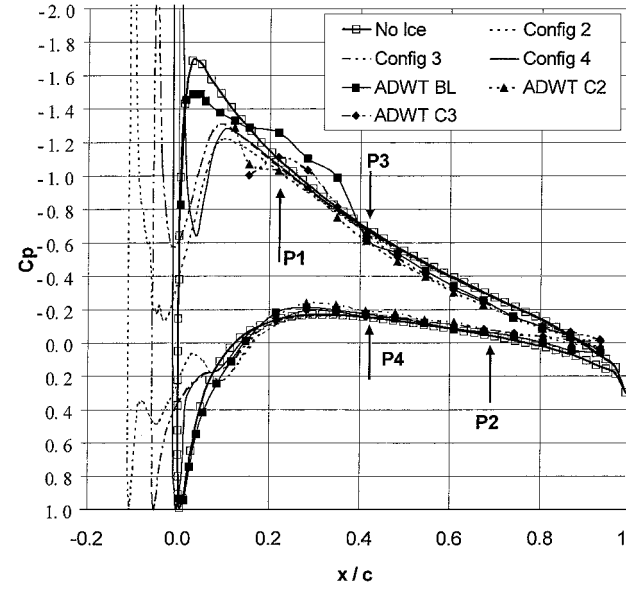

Fig. 10 LEWICE *Cp* **distributions for 5-deg angle of attack.**

LEWICE Analysis

The pressure distributions for the ice and no ice configurations were also studied using LEWICE.[3] This analysis provided insight into how the PLs, selected from the wind-tunnel data, provided nearly the same relationship between Cp_x and C_{LN}, regardless of ice shape. For angle of attacks from 0 to 5 deg, a pressure distribution was obtained for the ice and no ice configurations. An analysis of the data, for a given angle of attack, revealed the pressures at ports $P2$, $P3$, and $P4$ remained nearly unchanged. Port $P1$, on the other hand, varied as the ice configuration changed. This result is shown in Figs. 8–10. The locations of each port are indicated on the graphs. The pressure data in these graphs are presented in the form of the nondimensionalized pressure coefficient Cp.

As noted earlier, the model's airfoil section was not precisely that of an NACA 0018 airfoil. As can be seen in Figs. 8–10, the model pressure distribution is different from the LEWICE calculated values, forward of 40% chord. The ADWT data for the baseline no ice airfoil (ADWT BL), configuration 2 (ADWT C2), and configuration 3 (ADWT C3) are shown. Although the pressure distributions do not match at the leading edge, the response to the ice height has the same characteristics, as the hypothesis would predict.

Several observations can be made:

1) Port $P1$ has the greatest sensitivity to ice configuration and angle of attack because of its location on the upper surface and proximity to the leading edge of the airfoil. This location is very sensitive to the leading-edge shape and, thus, to the ice formation there. The remaining ports are insensitive to the leading-edge shape changes but remain sensitive to angle of attack and dynamic pressure changes, as is true for all of the ports. They serve to eliminate the effects of changes in dynamic pressure.

2) Because ports $P2$, $P3$, and $P4$ have nearly the same pressure for each ice shape, at a given angle of attack, their locations serve to adjust the relative percentage change caused by the change in $P1$, that is, scale the effect of $P1$.

3) The closer $P1$ is to the leading edge, the greater the pressure difference due to ice configuration will be, and therefore, the instrumentation will be more sensitive to the change in the wing leading-edge configuration.

Analysis of Icing Effect

Consider an aircraft that is in a cruise flight, holding a constant angle of attack. As ice accumulates on the leading edge of the wing, the Cp_x decreases. This is seen in the experimental data and the LEWICE analysis, as shown in Figs. 8–10. If the C_{LN} remained unchanged, this effect would result in a deviation from the baseline Cp_x vs C_{LN} calibration curve. This is shown in Fig. 10, by the vertical vector. In reality, an airplane flown at a constant angle of attack would have an increase in C_{LN} because of the decrease in stall

angle of attack associated with the leading-edge ice formation. This is shown in Fig. 11 by the horizontal vector. This brings the actual C_{LN}, obtained at the Cp_x measured with ice, back to the baseline calibration curve. In effect, the change in the Cp_x due to ice is offset by the change in the C_{LN} caused by the ice. As was pointed out in the preceding section, moving the ports will alter the effect of ice on the Cp_x. This would allow the designer to match the effect of the ice on the C_{LN}.

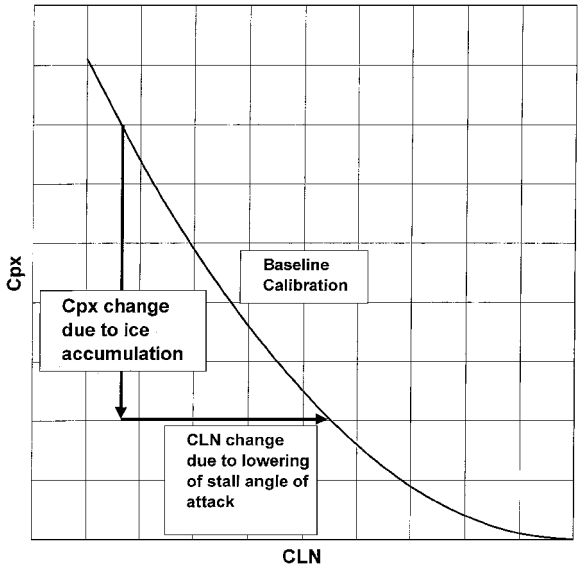

Fig. 11 C_{LN} vs Cp_x for a general calibration equation.

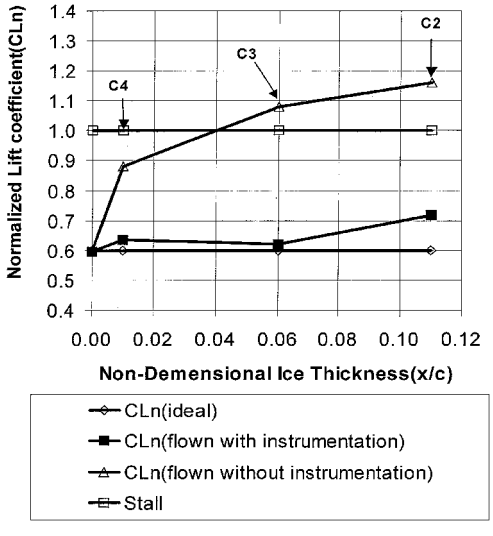

Fig. 12 Instrumentation comparison for an approach flown with an indicated $C_{LN} = 0.6$.

Instrumentation Evaluation

Figure 12 shows an evaluation of the system using the selected port locations. A $C_{LN} = 0.6$ was used because this would constitute a standard approach. The baseline relationship between C_{LN} vs Cp_x was used to calculate the C_{LN} as a function of Cp_x. The C_{LN} (ideal) represents the ideal, no error relationship. The C_{LN} (flown with instrumentation) represents the C_{LN} that would be indicated with ice formed on the leading edge, still using the baseline calibration. The C_{LN} (flown without instrumentation) represents the C_{LN} that would result if the angle of attack remained the same as it would be for the baseline at a $C_{LN} = 0.6$. This would be the result if a pilot were using a normalized lift indicator that obtained its inputs from angle of attack and flap deflection and not wing pressures. Under the worst tested case, the largest actual C_{LN} obtained would be 0.70, with the pressure-based instrumentation cockpit display indicating 0.6.

If a conventional C_{LN} system were used, the worst C_{LN} would be 1.17 (stalled), with the cockpit display indicating 0.6. This is not possible, and so in reality the aircraft control would have been lost before reaching this point.

Conclusions

The initial results show promise. Given that the relationships hold true for a wider range of ice shapes on typical wing airfoils, an instrumentation system could be made available to pilots. Such a system would give pilots information in icing conditions, well beyond that available today. Currently the pilot does not know how much lift coefficient is available in reserve. The pilot flying in icing conditions is in a test pilot role and could easily enter a stall, while flying airspeeds that would otherwise be normal. Even with deicing equipment, icing conditions exist that can have a serious impact on the airplane's aerodynamics. The system under development would allow the pilot to safely extract the airplane from the icing conditions and make a landing, knowing the margin from stall.

To prevent the pressure ports from being obstructed by ice, they would need to be heated. The ports would also need a provision to separate water and prevent blockage. The performance of the system with surface ice will need to be demonstrated. Future work should also include testing additional ice shapes and roughness on more typical wing airfoil sections tested experimentally and computationally. A computational method to predict the general PLs before wind-tunnel testing also needs to be developed. After verification of the two-dimensional work, three-dimensional testing over a variation of wing configurations and icing conditions will be needed.

References

[1]Hoadley, A., "Conversion of Wing Surface Pressures into Normalized Lift Coefficient," Society of Automotive Engineers Transactions, 790567, Nov. 1979.

[2]Hoadley, A., "Normalized Coefficient of Lift Indicator," U.S. Patent 4,235,104, Issued 11/25/80.

[3]Wright, W., "User Manual for the NASA Glenn Ice Accretion Code LEWICE," NASA CR-1999-209409, 1999.